Journal of Catalysis **195,** 360–375 (2000)
doi:10.1006/jcat.2000.2987, available online at http://www.idealibrary.com on IDEAL®

The Effect of Cation Type and H^+ on the Catalytic Activity of the Keggin Anion $[PMo_{12}O_{40}]^{3-}$ in the Oxidative Dehydrogenation of Isobutyraldehyde

Ji Hu and Robert C. Burns[1]

School of Biological and Chemical Sciences, The University of Newcastle, Callaghan 2308, Australia

Received March 23, 2000; revised July 4, 2000; accepted July 5, 2000

The oxidative dehydrogenation of isobutyraldehyde to methacrolein over $[PMo_{12}O_{40}]^{3-}$-containing catalysts has been shown to proceed through bulk catalysis-type II, which depends on the rates of diffusion of the redox carriers (H^+ and e^-) into the catalyst bulk. Variations in catalyst behaviour have been shown to change with the countercation and appear to be related to the polarizing ability of the cation, which can be represented by the ionic potential (charge/ionic radius). This, in turn, may indicate that the active site at the $[PMo_{12}O_{40}]^{3-}$ ion is close to an attendant countercation. For the alkali metal ions Li^+, Na^+, K^+, Rb^+, and Cs^+ as well as the (isoelectronic) ions of the series Cs^+, Ba^{2+}, La^{3+}, and Ce^{4+}, the studies have shown that conversion generally decreases with increasing ionic potential, while selectivity to methacrolein is less affected by changes in this property. However, the observed enhancement in selectivity to methacrolein and methacrylic acid in the case of Ce^{4+} is attributed to the ability of this cation to undergo reduction to Ce^{3+}, with the Ce^{4+}/Ce^{3+} couple likely acting to expedite the transfer of electrons between anions and hence into the bulk. Trends in the conversion and selectivities among the countercations Cs^+, NH_4^+, and $(CH_3)_4N^+$ show significant increases along this series, which is consistent with progressively increasing dissipation of the formal cationic charge. A mechanism for the oxidative dehydrogenation of isobutyraldehyde is proposed. The presence of H^+ enhances the activity of salts of $[PMo_{12}O_{40}]^{3-}$, most likely by protonation of the organic component, as little evidence from extended-Hückel molecular orbital calculations could be found for any reduction in the HOMO–LUMO gap of the anion upon protonation, which would make it easier to reduce the anion as part of the catalytic process.

Key Words: **isobutyraldehyde**; **heteropolyoxometalate**; **Keggin structure**; **bulk catalysis-type II.**

INTRODUCTION

Heteropolyoxometalate acids and salts are highly effective heterogeneous catalysts for the gas-phase selective oxidation of organic substrates. Examples include reactions such as the oxidative dehydrogenation of isobutyric acid and the oxidation of methacrolein, both of which yield methacrylic acid (1–5). Methacrylic acid is, in turn, reacted with methanol to yield methyl methacrylate, an extremely important acrylic monomer, which is then polymerized to give poly(methyl methacrylate). Heteropolyoxometalates are also active acid catalysts, and processes based both on their redox and acid–base properties have found commercial applications (3–5).

The study of heteropolyoxometalates as oxidation–reduction catalysts has involved primarily Keggin-based structures, principally $[PMo_{12}O_{40}]^{3-}$, as well as substituted species involving replacement of one or more framework Mo(VI) by V(V) (3–5). The geometry of the (α-)$[PMo_{12}O_{40}]^{3-}$ ion consists of a central tetrahedrally coordinated phosphorus atom surrounded by four groups of three edge-sharing octahedra (i.e., Mo_3O_{13} subunits), which are in turn linked to each other and to the central PO_4 tetrahedron by shared oxygen atoms at the vertices (6). Some studies have also included the related Dawson structure ion $[P_2Mo_{18}O_{62}]^{6-}$, which is formed by joining two "$[PMo_9O_{31}]^{3-}$" monomeric units, the latter being formed by loss of three MoO_3 groups, one each from three adjacent Mo_3O_{13} subunits of the Keggin structure anion (7).

The majority of studies of heteropolyoxometalates as oxidation–reduction catalysts have concerned the oxidative dehydrogenation of isobutyric acid and the oxidation of methacrolein (3–5), although the oxidative dehydrogenation and oxidation of isobutane have recently received considerable attention (8, 9), as has the partial oxidation of methane using N_2O as the oxidant (10–13). Methacrolein can be prepared by the oxidative dehydrogenation of isobutyraldehyde, which is formed as a by-product of the oxo synthesis of propene to yield *n*-butyraldehyde. While the oxidative dehydrogenation of isobutyraldehyde has been investigated, it is not as well studied as that of isobutyric acid. Thus, for example, isobutyraldehyde has been converted to methacrolein over iron phosphate at 400°C with a conversion/selectivity of 88%/68% (14), over $H_3PMo_{12}O_{40}$ (containing Sb, Zn, and Cr) at 295°C, 88.3%/40.8% (also

[1] Dr. R. C. Burns, School of Biological and Chemical Sciences, The University of Newcastle, Callaghan, New South Wales, Australia, 2308. E-mail: csrb@paracelsus.newcastle.edu.au. Telephone: +61-2-49215479.

0021-9517/00 $35.00

with 6.9% methacrylic acid) (15), and over $H_3PMo_{12}O_{40}$ (containing Zr, V, and Cs) at 310°C, 100%/76.5% (also with 8.9% methacrylic acid) (16). Other studies have included the effects of the substitution of La^{3+} for H^+ in $H_4PVMo_{11}O_{40}$ (17) and the effect of changing the central heteroatom in the Keggin anion from P(V) to As(V) (18). There has been, however, no comprehensive study yet undertaken equivalent to those of the oxidative dehydrogenation of isobutyric acid over various salts of the $[PMo_{12}O_{40}]^{3-}$ ion (1, 19, 20) or of the effects of added H^+ (21). The present study details such an investigation of the oxidative dehydrogenation of isobutyraldehyde and allows comparisons with the studies of isobutyric acid under similar conditions. Salts of the $[PMo_{12}O_{40}]^{3-}$ ion were used in this work as this avoids the complications that are found in the case of, for example, $[PVMo_{11}O_{40}]^{4-}$, which loses VO^{2+} upon thermal treatment or during catalysis with isobutyric acid (22). In this study, variations in the countercations are examined, and suggestions are made concerning the mechanism of the oxidative dehydrogenation process of isobutyraldehyde and isobutyric acid as well as the role played by the presence of H^+.

EXPERIMENTAL

Preparation and Characterization of Salts of the $[PMo_{12}O_{40}]^{3-}$ Anion

Phosphomolybdic acid, $H_3[PMo_{12}O_{40}] \cdot 23H_2O$ (water content determined by TGA), and $(NH_4)_3[PMo_{12}O_{40}]$ were obtained commercially (Ajax/Univar and Aldrich, respectively). The alkali metal salts of the $[PMo_{12}O_{40}]^{3-}$ ion were prepared according to the method of Tsigdinos (23), by addition of a stoichiometric amount (3:1 mole ratio) of an alkali metal carbonate to a concentrated aqueous solution of $H_3[PMo_{12}O_{40}]$ and isolation of the yellow product, in the case of the K^+, Rb^+, and Cs^+ salts, by filtration and drying at room temperature. The aqueous-soluble Li^+ and Na^+ salts were isolated by removal of water at ~50°C. The insoluble $[PMo_{12}O_{40}]^{3-}$ salts, i.e., K^+, Rb^+, and Cs^+, and the NH_4^+ salt were stirred subsequently for 30 min with 0.1 mol dm^{-3} solutions of their respective MCl (M = alkali metal) or NH_4Cl to remove any extraneous H^+ included in their structures (24). The samples were filtered, washed with a little water, and dried at ~50°C. The Ba^{2+} and La^{3+} salts were obtained by reaction of the appropriate amounts of their metal carbonates with $H_3[PMo_{12}O_{40}]$ and removal of the water as in the case of the Li^+ and Na^+ salts. The Ce^{4+} salt was obtained by addition of a solution of cerium(IV) sulfate hydrate (Aldrich, cerium content 30% minimum) to one of $H_3[PMo_{12}O_{40}]$, followed by the addition of the appropriate amount of $BaCO_3$ to precipitate insoluble $BaSO_4$. The latter was removed by filtration and the orange-yellow Ce^{4+} salt isolated by evaporation of water at ~50°C. The mixed cation phases $(Cs_nH_{3-n})[PMo_{12}O_{40}]$ (with n nominally equal to 1, 2, and 2.5) were prepared by addition of the appropriate amounts of aqueous Cs_2CO_3 to solutions of $H_3[PMo_{12}O_{40}]$, followed by removal of water at ~50°C, while the Me_4N^+ and $^nBu_4N^+$ salts were obtained by addition of a stoichiometric amount of Me_4NCl or $^nBu_4NBr$ to concentrated aqueous solutions of $H_3[PMo_{12}O_{40}]$, followed by isolation of the yellow products by filtration and drying at room temperature. The infrared spectra of all compounds and the ^{31}P NMR spectrum of $(Me_4N)_3[PMo_{12}O_{40}]$ and $(^nBu_4N)_3[PMo_{12}O_{40}]$ ($\delta = -2.73$ and -2.74 ppm, respectively, from 85% H_3PO_4; DMSO solvent) were in agreement with published data (25).

Samples of $(NH_4)_3[PMo_{12}O_{40}]$ with a low surface area were prepared by two methods: (1) the thermal decomposition of $(^nBu_4N)_3[PMo_{12}O_{40}]$ at 300°C in air and (2) by direct reaction of anhydrous $H_3[PMo_{12}O_{40}]$ with excess gaseous NH_3 (BOC) at 0°C, followed by heating at 100°C to ensure complete reaction. The thermal decomposition of $(^nBu_4N)_3[PMo_{12}O_{40}]$ to $(NH_4)_3[PMo_{12}O_{40}]$ was accomplished by static heating in an air atmosphere at 300°C for 1 week. This resulted in a yellow-brown material, which upon washing with distilled water produced a yellow compound. The infrared spectra of both materials indicated that the $[PMo_{12}O_{40}]^{3-}$ ion had remained intact, while the X-ray powder diffraction patterns were identical to that of an authentic sample of $(NH_4)_3[PMo_{12}O_{40}]$. Chemical analyses of the commercial sample, that obtained by thermal decomposition of $(^nBu_4N)_3[PMo_{12}O_{40}]$, and that obtained by reaction of anhydrous $H_3[PMo_{12}O_{40}]$ with NH_3 gave the following results: %N, 2.03, 1.55, and 2.24, respectively (theoretical value of 2.24%); %H, 0.69, 0.59, and 0.60, respectively (theoretical value of 0.69%). The sample obtained by thermal decomposition also contained 0.15% C, indicating that the $^nBu_4N^+$ ion had not completely decomposed or that some carbon-based impurity was still present in the sample.

To test for the presence of H^+ in soluble catalysts (which has an enhancing effect on the oxidative dehydrogenation of isobutyraldehyde), a UV–visible spectroscopic procedure using the base form of the indicator bromothymol blue (sodium salt, Aldrich, ~90% dye content) in *N,N*-dimethylformamide (DMF) (Aldrich, 99.8%, anhydrous, dried over type 4A molecular sieves) was employed. Any H^+ that may have been retained following isolation of the neutral salts of the $[PMo_{12}O_{40}]^{3-}$ ion or formed during preparation by the hydrolysis reaction given below (Eq. [1]) can be measured spectrophotometrically in solution by conversion of the base form of bromothymol blue ($\lambda_{max} = 636$ nm, $\varepsilon = \sim 45{,}000$ L mol^{-1} cm^{-1}) into its acid form.

$$[PMo_{12}O_{40}]^{3-} + 3H_2O \leftrightarrow [PMo_9O_{31}]^{3-} + 3[HMoO_4]^- + 3H^+. \quad [1]$$

In organic solvents such as acetone and ethanol, the pK_1,

pK_2, and pK_3 values for the $H_3[PMo_{12}O_{40}]$ range from 2.0 to 5.3 (26) and the various protonated forms of $[PMo_{12}O_{40}]^{3-}$ will be stronger acids in the more basic solvent DMF. Bromothymol blue has pK_a values of 7.2 and 12.4 in water and methanol, respectively (27), and ~10 in DMF [estimated from data provided in Ref. (27)] and thus will be easily protonated. For the determination of the amount of H^+ in soluble catalysts, known concentrations (2.0×10^{-5} mol dm^{-3} in $[PMo_{12}O_{40}]^{3-}$) of the Li^+ and Na^+ salts (calcined at 300°C for 6 h) were prepared and the reduction in absorbance of the base form of the indicator at 636 nm (using an initial concentration of the sodium salt of bromothymol blue of 2.0×10^{-4} mol dm^{-3}) was measured relative to a solution of the same concentration of the indicator that did not contain the catalyst. At this wavelength any absorbance from the acid form of the indicator ($\lambda_{max} = 403$ nm) and from the $[PMo_{12}O_{40}]^{3-}$ ion (absorbance occurs at wavelengths less than ~500 nm) do not interfere with the measurement. All solutions were prepared under nitrogen and the spectra obtained using sealed cells to eliminate water. In both cases the reduction in absorbance was used to generate a H^+ concentration and then, using the above equation (also noting that $[HMoO_4]^-$ will be a strong acid in DMF), this was expressed as the amount of $[PMo_{12}O_{40}]^{3-}$ hydrolysed during preparation. Initial values of absorbance were used to avoid the possibility of any further reactions, such as reformation of $[PMo_{12}O_{40}]^{3-}$ upon standing in solution. The results indicated that both salts experienced a similar extent of hydrolysis of $[PMo_{12}O_{40}]^{3-}$ during preparation (8% and 5% for the Li^+ and Na^+ salts, respectively).

All (neutral) salts used in this study, $H_3[PMo_{12}O_{40}]$, and the two samples of $(NH_4)_3[PMo_{12}O_{40}]$ prepared by the alternative methods described above were also tested using the standard approach for solid acids (28) with the Hammett indicators 4-(phenylazo)diphenylamine (Aldrich, 97%) and dicinnamalacetone (Aldrich, 98%), which cover a range of sites of different acid strengths. Samples were tested following calcination at 300°C for 6 h or drying over silica gel under vacuum. All catalysts showed evidence of surface acidity with 4-(phenylazo)diphenylamine (p$K_a + 1.5$) as well as with dicinnamalacetone (p$K_a - 3.0$). The water-soluble catalysts exhibited strong surface acidity based on colouration with both indicators. However, the water-insoluble species that had been cation exchanged as described above, with the exception of the commercial sample of $(NH_4)_3[PMo_{12}O_{40}]$, appeared to produce less intense colouration. This was noticably so for the Rb^+ and Cs^+ salts, despite their generally greater surface areas, and suggests that there was less H^+ present on the surfaces of these two catalysts, although this does depend on the number of protons at the particular acid strength of the site. The samples of $(NH_4)_3[PMo_{12}O_{40}]$ prepared by thermal decomposition of $(^nBu_4N)_3[PMo_{12}O_{40}]$ and by reaction of $H_3[PMo_{12}O_{40}]$ with NH_3 both showed strong surface reactions with the two Hammett indicators. Using a scale from 0 to 4, with 0 representing no response to the Hammett indicators and 4 that of $H_3[PMo_{12}O_{40}]$, all catalysts were assigned values of ≥3, while both the Rb^+ and Cs^+ salts had a value of 1.

Thermogravimetric analyses were performed on a Stanton Redcroft TG-750 instrument coupled to a Eurotherm Model 94 temperature controller. Sample masses of about 10 mg were used with a heating rate of 10°C/min in a static air atmosphere. Infrared spectra were recorded on a Bio-Rad FTS-7 Fourier-transform spectrophotometer, with samples mounted as KBr discs. UV–visible spectra were obtained using a Hitachi U-2000 spectrophotometer with 1-cm cells. X-ray powder diffraction was performed on a Philips PW1700 Automated Powder Diffractometer System 1, employing graphite-monochromated Cu $K\alpha$ radiation. Scanning electron microscopy was performed on a Philips XL-30 scanning electron microscope operating at 15 kV. Solution ^{31}P NMR spectra were recorded with a Bruker AVANCE DPX-300 spectrometer operating at 121.49 MHz. The reference used was external 85% H_3PO_4. Solid-state ^{31}P NMR spectra were obtained with a Bruker MAS-300 spectrometer operating at 121.49 MHz. Samples (~150 mg) were contained in a partially stabilized zirconia tube fitted with a Kel-F cap and were spun at a rate of 10 kHz. The reference used was solid $(NH_4)H_2PO_4$. Surface area measurements were made by the BET method using nitrogen adsorption on a Micromeritics ASAP 2400 instrument. All samples were prepared using an identical method to that described for the catalysis samples (see below) and were degassed at 300°C prior to measurement.

Catalysis and Analysis of Products

The catalytic activities of the various salts of the $[PMo_{12}O_{40}]^{3-}$ anions toward the gas-phase oxidative dehydrogenation of isobutyraldehyde were carried out using a conventional flow fixed-bed reactor (a 30-cm long quartz tube with an internal diameter of 4 mm). Reactions were conducted at atmospheric pressure and at temperatures of 275 and 300°C following an initial temperature effect study of both $(NH_4)_3[PMo_{12}O_{40}]$ and $K_3[PMo_{12}O_{40}]$ at 275, 300, 325, and 350°C. The feed gas consisted of 1% isobutyraldehyde (Aldrich, 98%, which was freshly distilled under nitrogen and transferred to the catalysis system saturator using a gas-tight syringe) and 3% oxygen, with a nitrogen balance. The saturator was held at 0°C using an ethanol–water cold bath to ensure a constant vapour pressure of isobutyraldehyde during each catalysis study. Typical catalyst masses of 0.35 g (~0.21 ml) or 0.20 g (~0.13 ml) were used (after allowing for loss of water), which when combined with a flow rate of 150 cm^3 min^{-1} gave residence times of ~0.09 and ~0.05 s, respectively, assuming plug flow. This corresponds to a W/F (weight of catalyst per total flow rate) of 0.14 and 0.08 g s ml^{-1}, respectively. Catalysts samples were prepared

by compressing the powdered catalyst at a pressure of 1.7 ton cm^{-2}, which was broken up and passed through a series of sieves, with the fraction 40–80 mesh used for the studies. The catalyst samples were loaded between silica wool plugs in the quartz reactor tube. Samples were calcined at 10°C above the maximum temperature to be employed in the study for 2 h under a flow of nitrogen containing 3% oxygen.

Following the establishment of a steady state in each case (~4 h), which was monitored by the IR detection and analysis of both CO and CO_2, the condensable gaseous products, methacrolein, acetone, methacrylic acid, and unreacted isobutyraldehyde, were collected in an acetone–dry ice cold bath for a period of 30 min and used as representative of the conversion and selectivity for the sampling time. The water produced during the reaction was not determined. No evidence for the formation of nitriles, such as isobutyronitrile and methacrylonitrile, was found with NH_4^+ as the cation, although species of this type have been observed during the oxidative dehydrogenation of isobutyric acid (16). The above products were analysed by gas chromatography (3 wt% FFAP and 7 wt% OV-17 on acid-washed Chromosorb-W). The carbon balance was routinely in the range 90–100%. The conversion percentage of isobutyraldehyde was calculated as 100[1-(mol of unreacted isobutyraldehyde/mol of isobutyraldehyde introduced)], while the selectivities percentages of the various products were determined as 100(mol of component *i*/total number of mol of products).

Extended-Hückel Molecular Orbital Calculations

Extended-Hückel molecular orbital calculations were performed using the package described by Mealli and Proserpio (29) (Version 4.0, 1994), with the extended-Hückel parameters, i.e., Coulomb integrals, H_{ii} (eV), and Slater exponents (ξ), taken from the values provided in the package. The Wolfsberg–Helmholtz constant was set to 1.75. The geometry of the $[PMo_{12}O_{40}]^{3-}$ ion used in the calculation was taken from the structure of $H_3[PMo_{12}O_{40}] \cdot 30H_2O$ (30, 31). For calculations on the NH_4^+ ion the N–H distance was taken as 1.02 Å, while for the Me_4N^+ ion the N–C and C–H distances were 1.45 and 1.05 Å, respectively.

RESULTS AND DISCUSSION

I. Catalysis and Supporting Studies

A. Effect of Temperature over $(NH_4)_3[PMo_{12}O_{40}]$ and $K_3[PMo_{12}O_{40}]$

Initial investigations into the appropriate conditions under which to study the type of catalysis and the effects of cation variations on the oxidative dehydrogenation of isobutyraldehyde employed the salts $(NH_4)_3[PMo_{12}O_{40}]$ and $K_3[PMo_{12}O_{40}]$. The compounds are isostructural, with very similar unit cell dimensions and surface areas (see below). In both cases a steady state was not achieved for some 4 h following initiation of catalysis. This was also observed for all of the remaining salts in subsequent studies. The results of temperature dependence studies (conversion, selectivity, and efficiency percentage) for both compounds are given in Figs. 1 and 2 for the range 275 to 350°C. The temperature for the most efficient (%) formation of methacrolein (MAL) plus methacrylic acid (MAA) is given by the expression

$$\text{efficiency (\%)} = [(\text{\% conversion}) \times (\text{\% selectivity to MAL} + \text{MAA})]/100.$$

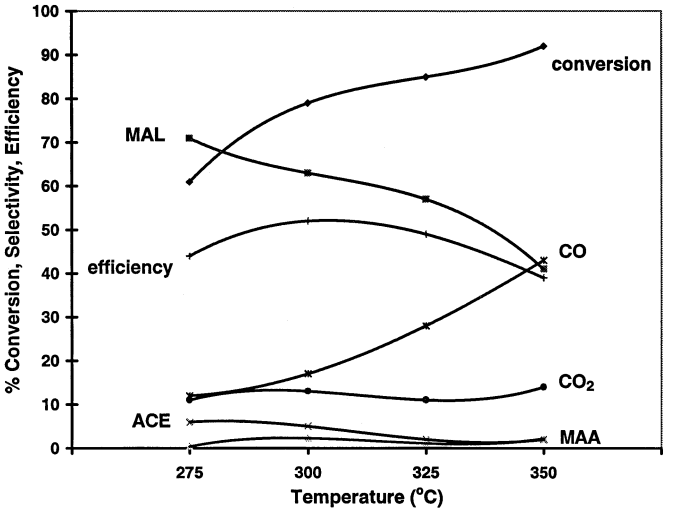

FIG. 1. Effect of temperature on the oxidative dehydrogenation of isobutyraldehyde over $(NH_4)_3[PMo_{12}O_{40}]$: 1% isobutyraldehyde, 3% oxygen; W/F 0.08 g s ml^{-1}.

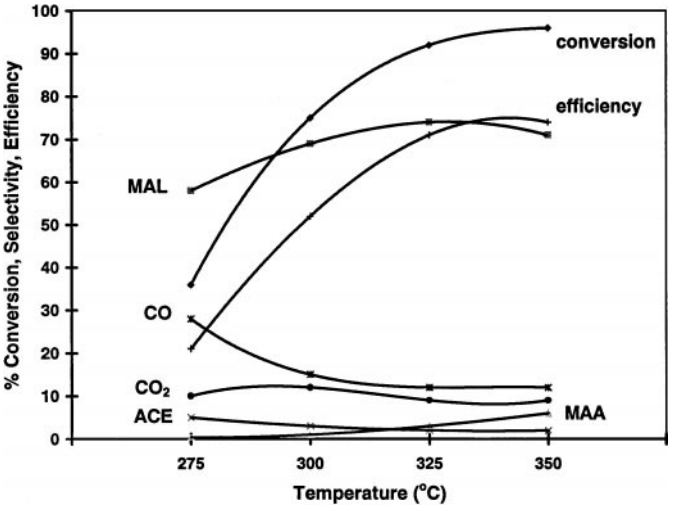

FIG. 2. Effect of temperature on the oxidative dehydrogenation of isobutyraldehyde over $K_3[PMo_{12}O_{40}]$: 1% isobutyraldehyde, 3% oxygen; W/F 0.08 g s ml^{-1}.

For $(NH_4)_3[PMo_{12}O_{40}]$ and $K_3[PMo_{12}O_{40}]$ the efficiencies peaked at ~305 and ~340°C, respectively. For the former salt, although methacrolein and methacrylic acid formation decreased with increasing temperature, conversion increased, leading to the most efficient formation of the desired products at ~305°C. Interestingly, the CO_2 selectivity changed little with temperature, suggesting that complete oxidation of the products was not a major competitive pathway over the temperature range studied. In contrast, that of CO increased markedly, which is the cause of the decrease in methacrolein selectivity with increasing temperature. The selectivity of acetone paralleled that of methacrolein. These results suggest that methacrolein, acetone, and CO are linked through a common intermediate in the mechanism of formation of the product species.

For $K_3[PMo_{12}O_{40}]$, the selectivity of methacrolein increased with increasing temperature until ~325°C, subsequently followed by a slight decrease, while that of methacrylic acid progressively increased with increasing temperature. Combined with an increasing conversion at higher temperatures, this led to a maximum efficiency for methacrolein and methacrylic acid production at ~340°C. Again CO_2 selectivity was essentially constant, but the CO and acetone selectivities both decreased with increasing temperature as methacrolein increased and the former became effectively constant above ~325°C. Once again, this suggests a link between methacrolein, acetone, and CO formation, as indicated above for $(NH_4)_3[PMo_{12}O_{40}]$.

Comparison of the trends in conversion and the selectivities of the products with temperature for these two (isostructural) catalysts, particularly for methacrolein, indicates different behaviour, despite the presence of the same $[PMo_{12}O_{40}]^{3-}$ ion. This suggests that the countercation plays an active role in the conversion and selectivity trends of compounds of the $[PMo_{12}O_{40}]^{3-}$ ion. Similar conclusions have been drawn regarding the oxidative dehydrogenation of isobutyric acid over a range of $[PMo_{12}O_{40}]^{3-}$-containing catalysts with varying countercations (1, 20). All subsequent studies were performed at 275 and 300°C, to the lower side of the temperature of maximum efficiency of both $(NH_4)_3[PMo_{12}O_{40}]$ and $K_3[PMo_{12}O_{40}]$. Most of the other alkali metal cations behaved in a manner similar to that of the K^+ salt, while $(CH_3)_4N^+$ behaved like the NH_4^+ salt. Some salts appeared intermediate in behaviour between these extremes, although these latter conclusions are based only on data at 275 and 300°C.

B. *Effect of Differences in Surface Area over $(NH_4)_3[PMo_{12}O_{40}]$*

(i) Catalysis studies. It has been established in previous studies that the oxidative dehydrogenation of isobutyric acid over salts of the $[PMo_{12}O_{40}]^{3-}$ ion occurs by bulk catalysis-type II (3–5). This is different from conventional heterogeneous catalysis over a solid, where the reaction takes place at the two-dimensional surface of the solid catalyst, with the reaction rate proportional to the surface area. In bulk catalysis-type II, while the reaction still occurs at the catalyst surface, the inner bulk of the catalyst plays a role, with the contribution depending on the rate of the catalytic reaction relative to the rates of diffusion of the redox carriers (H^+ and e^-) into the bulk. In the ideal (limiting) case, the rate is proportional to the volume (or mass) of the catalyst, although some dependence on surface area may be observed, depending on the relative rates of the above processes. It is likely that the oxidative dehydrogenation of isobutyraldehyde operates by bulk catalysis-type II, as does the oxidative dehydrogenation of isobutyric acid, given the similarities in their structures.

One way to test whether or not surface area is important in the oxidative dehydrogenation of isobutyraldehyde, and hence establish the type of catalysis operating, is by the preparation of the same catalyst material with vastly different surface areas, followed by an examination of their relative activities under identical conditions. For this purpose, $(NH_4)_3[PMo_{12}O_{40}]$, likely formed by direct precipitation (commercial sample, Aldrich), was compared with materials prepared by two other different synthetic approaches. These included syntheses involving the thermal decomposition of $(^nBu_4N)_3[PMo_{12}O_{40}]$ (32) and by direct reaction of anhydrous $H_3[PMo_{12}O_{40}]$ with excess NH_3 gas. For the analogous tungstate system it has been reported previously (33) that anhydrous $H_3[PW_{12}O_{40}]$ reacts quantitatively with NH_3 to produce $(NH_4)_3[PW_{12}O_{40}]$, but no studies have been reported for $H_3[PMo_{12}O_{40}]$. The commercial sample of $(NH_4)_3[PMo_{12}O_{40}]$, following ion exchange (see above), had a measured surface area of 120 $m^2\,g^{-1}$. For the thermally produced sample, the precursor, $(^nBu_4N)_3[PMo_{12}O_{40}]$, had a surface area of 1.5 $m^2\,g^{-1}$. Following thermal decomposition, the product had an IR spectrum and XRD pattern identical to those of an authentic sample of $(NH_4)_3[PMo_{12}O_{40}]$, but with a surface area of only 5.3 $m^2\,g^{-1}$. Similarly, the material produced by direct reaction of the anhydrous acid (1.2 $m^2\,g^{-1}$) with gaseous NH_3 would not be expected to increase greatly as NH_3 is able to penetrate the interanionic voids and react with the H^+ to give NH_4^+ ions. The resulting material again had an IR spectrum and XRD pattern identical to those of an authentic sample of $(NH_4)_3[PMo_{12}O_{40}]$, with a surface area of 7.0 $m^2\,g^{-1}$. The catalysis results for all three samples of $(NH_4)_3[PMo_{12}O_{40}]$ are given in Table 1. Some slight differences in the conversion percentage of isobutyraldehyde are observed, with a decreased conversion for the lower surface area materials. However, the changes in the rates and conversion percentages are relatively small (less than a factor of 2) compared to the changes in the surface areas of the samples, which vary by a factor of ~20. Thus, surface area does not appear to be a major factor in controlling the rate of this reaction and strongly indicates that

TABLE 1

Effect of Surface Area of $(NH_4)_3[PMo_{12}O_{40}]$ on the Oxidative Dehydrogenation of Isobutyraldehyde

Catalyst preparation	Surface area ($m^2\,g^{-1}$); pore volume ($cm^3\,g^{-1}$)	Temp. (°C)	% Conv.	Rate (10^4 mol $min^{-1}\,g^{-1}$)	% Selectivity[a] MAL	MAA	ACE	CO	CO_2
Commercial sample	120; 0.126	275	61	1.88	71	<1	6	10	12
		300	81	2.50	62	2	5	18	13
Thermal decomp.	5.3; 0.012	275	38	1.17	64	<1	4	19	12
		300	48	1.48	66	1	3	16	14
Acid + excess NH_3	7.0; 0.028	275	44	1.36	70	<1	4	15	10
		300	63	1.95	67	1	3	16	13

Note. Mass of catalyst, 0.20 g; W/F = 0.08 g s ml^{-1}.

[a] MAL, methacrolein; MAA, methacrylic acid; ACE, acetone.

bulk catalysis-type II is operating. The observed differences in conversion and selectivities percentages are likely attributable to varying amounts of residual H^+ in the samples (caused by either incomplete removal of H^+ following exchange with NH_4Cl, formation of H^+ during thermal decomposition, or incomplete neutralization of H^+ with NH_3), which has an enhancing effect on the catalytic activity of salts of the $[PMo_{12}O_{40}]^{3-}$ ion. This is discussed in more detail below.

Comparison of the selectivity percentage data for the three samples indicates that the selectivity to methacrolein varies from 62 to 71% (data for both temperatures), with no dependence on the differences in the surface areas of the catalysts. The high surface area commercial sample produced slightly more methacrylic acid, but this is consistent with the subsequent oxidation of the initial product methacrolein to methacrylic acid over these types of catalysts, which is a reaction that is known to depend on the surface area of the catalyst (21). There appears to be no trends in the selectivities to acetone, CO, or CO_2 with differences in surface area. The selectivity to acetone decreased with increasing temperature, as has been observed previously (Fig. 1), while those to CO and CO_2 showed slight variations.

(ii) SEM, pore volume, and pore size studies. The SEM micrographs of the three samples of $(NH_4)_3[PMo_{12}O_{40}]$ used in the above studies are shown in Fig. 3. The commercial sample (probably precipitated) that had been ion-exchanged with NH_4Cl (Fig. 3a) exhibited small, spherical crystals ranging from ~0.1 to ~0.5 μm in diameter. This morphology likely reflects the isotropic nature of crystal growth of the compound from solution (which has a cubic unit cell, see below), thus resulting in an almost spherical shape. The range and small sizes of the crystals contribute to the high surface area of the compound (120 $m^2\,g^{-1}$). In contrast, both materials obtained by nonprecipitative methods (Figs. 3b and 3c, respectively) show large irregular block-like crystals of varying sizes, which are effectively identical to the original crystals of the parent species from which they were formed. Using a calculated crystallographic density for $(NH_4)_3[PMo_{12}O_{40}]$ of 3.93 g cm^{-3}, together with an average diameter for the spherical crystals of ~0.2 μm for the high-surface area material and $5 \times 10 \times 10$ μm for the dimensions of the block-like crystals found for both low surface area samples, the respective calculated surface areas are ~4 and ~0.2 $m^2\,g^{-1}$. These will be lower limits as they assume that the surfaces are smooth and likely will be a factor of 2 or 3 larger, allowing for roughness. Thus, there is an ~20-fold increase in surface area in going from the low to the high surface area materials from these calculations. Both calculated values suggest that all three samples have some internal pore structure, particularly the commercial sample. The pore volume, obtained from BET measurements, of the high surface area sample was 0.126 $cm^3\,g^{-1}$, while those of the other samples were 0.012 and 0.028 $cm^3\,g^{-1}$ (Table 1). Precipitated (high surface area) $(NH_4)_3[PMo_{12}O_{40}]$ is known to be a microporous material and has previously been reported to have a surface area of 193 $m^2\,g^{-1}$, with a mean micropore radius of 13 Å, and an average mesopore radius of 35 or 45 Å, depending on the pore shape (cylindrical or slit models, respectively) (34). The pore size analysis of the high surface area salt in the present study yielded an average mesopore diameter of 39 Å (cylindrical model), which is in reasonably good agreement with the reported data, while those of the two low surface area salts were 142 and 189 Å for $(NH_4)_3[PMo_{12}O_{40}]$ prepared by thermal decomposition of $(^nBu_4N)_3[PMo_{12}O_{40}]$ and by direct reaction of anhydrous $H_3[PMo_{12}O_{40}]$ with excess NH_3 gas, respectively. The low surface areas of the latter compounds, with their low pore volumes and large pore diameters, reflect the original crystal morphologies of the compounds from which they were formed. However, the slight increases in surface areas on their formation suggest that some pore structure may have developed during the rearrangement of the

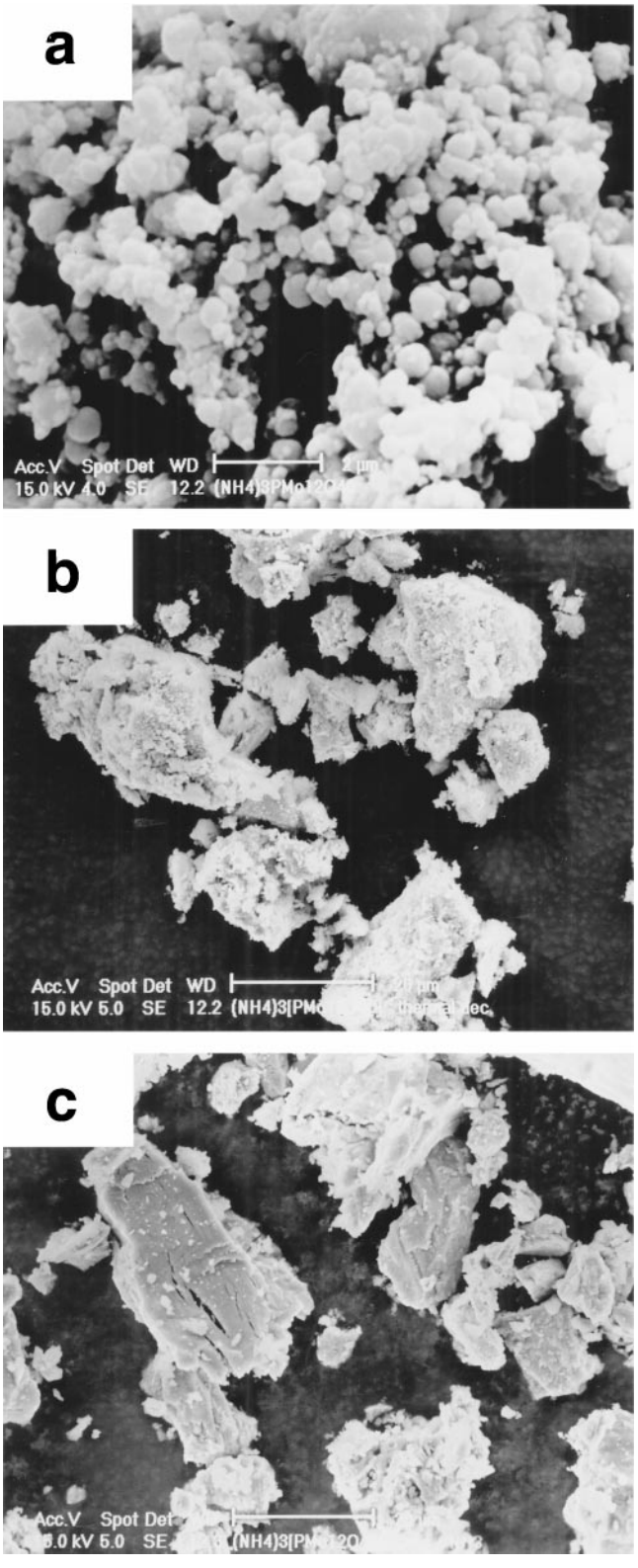

FIG. 3. SEM images of $(NH_4)_3[PMo_{12}O_{40}]$: (a) commercial sample, Aldrich (precipitated) (scale bar, 2 μm); (b) synthesised by the thermal decomposition of $(^nBu_4N)_3[PMo_{12}O_{40}]$ in air at 300°C (scale bar, 20 μm); (c) synthesised by the direct reaction of $H_3[PMo_{12}O_{40}]$ and excess gaseous NH_3 (scale bar, 20 μm).

atoms upon thermal decomposition of $(^nBu_4N)_3[PMo_{12}O_{40}]$ and upon reaction of anhydrous $H_3[PMo_{12}O_{40}]$ with excess NH_3. Thus, examination of the SEM images in Figs. 3b and 3c show extensive cracking and evidence of holes leading to the inner regions of the crystals.

C. Effect of Cation Size and Charge on the Oxidative Dehydrogenation of Isobutyraldehyde [Li^+, Na^+, K^+, Rb^+, and Cs^+; Ba^{2+}, La^{3+}, and Ce^{4+}; NH_4^+ and $(CH_3)_4N^+$ Salts]

To investigate the effects of varying the countercation on the oxidative dehydrogenation of isobutyraldehyde (Table 2), an initial series of compounds of the $[PMo_{12}O_{40}]^{3-}$ ion containing cations of the same charge but varying ionic radii (Li^+, Na^+, K^+, Rb^+, and Cs^+) were examined.

When precipitated from solution, the insoluble K^+, Rb^+, and Cs^+ salts, and the NH_4^+ salt, crystallize with a cubic unit cell, with $a = \sim 11.7$ Å, space group $Pn3m$, and $Z = 2$ (35). However, the soluble Li^+ and Na^+ salts, following removal of solvent, can have different structures. The former had an XRD pattern somewhat similar to that of $H_3[PMo_{12}O_{40}] \cdot 23H_2O$, while the pattern of the latter indicated at least two components, the major component having the above cubic unit cell and a second, more complex pattern, showing some similarities to that of the Li^+ salt. All alkali metal salts are hydrated to varying extents, as shown by the results of TGA studies, which are given in Table 3. The Li^+ salt is the most hydrated while the salts of the other alkali metal cations, and the NH_4^+ salt, all have a similar extent of hydration. Thermogravimetric analysis results indicated that the K^+, Rb^+, Cs^+, and NH_4^+ salts lost this water before 100°C, the Na^+ salt at ~170–200°C, while the Li^+ salt continuously lost water up to ~400°C. At 300°C both the Li^+ and Na^+ salts transform over a period of 4 to 6 h completely into phases that have the above cubic unit cell, with the Li^+ salt the slower to undergo this transformation. Thus, all five (anhydrous) alkali metal salts and the NH_4^+ salt are isostructural. The actual unit cell dimensions are also given in Table 3 from the results of a Rietvelt profile analysis and not surprisingly show an increase in value with increasing size of the alkali metal cation, except for a discontinuity between the Na^+ and K^+ salts. The unit cell size of the NH_4^+ salt is about the same as that of the Rb^+ salt, reflecting their similar cationic radii, while the origin of the discontinuity between the Na^+ and K^+ salts may be related to expansion of the lattices of the (water-soluble) Li^+ and Na^+ salts following adsorption of water from the air upon standing at room temperature.

Examination of the SEM micrographs of the Li^+, Na^+, K^+, Rb^+, and Cs^+ salts (all calcined at 300°C for 6 h) indicate several features. For the soluble Li^+ and Na^+ salts the crystals were, in general, large irregularly shaped blocks, which varied in size from ~2 to 20 μm. However, for the insoluble K^+ and Rb^+ salts, the crystals were considerably

smaller, with a range of 0.1 to ~1 μm, fairly spherical in shape and similar to the crystals of the commercial sample of $(NH_4)_3[PMo_{12}O_{40}]$ (Fig. 3). This again likely results from isotropic growth from solution. Their surfaces appeared to be free of defects. The Cs^+ salt had a similar crystal shape to that of the K^+ and Rb^+ salts, but the crystal sizes were even smaller, with a range of 0.05 to 0.3 μm. Thus, the significant differences in the crystal sizes, resulting from their varying solubilities, contribute to the observed differences in surface area for both the Li^+ and Na^+ salts compared to those of the K^+, Rb^+, and Cs^+ salts (Table 3), as described above for the NH_4^+ salts.

For the series of alkali metal cations the catalysis results are given in Table 2. These results show that an increased conversion percentage occurred at the higher temperature, as expected, along with an increased selectivity percentage to methacrolein (and methacrylic acid). The conversion percentage generally follows the sequence $Li^+ < Na^+ < K^+$, with both the Rb^+ and Cs^+ salts less active than the K^+ salt. At first sight there appears to be little trend in either the conversion percentage or the selectivity percentage to methacrolein and methacrylic acid from monotonically changing the cation and hence any dependence on a property such as the ionic potential of the cation. The ionic potential is given by the charge/cation radius (Z/r) and provides a measure of the polarizing ability of the cation and hence the ability to influence electron density at neighbouring atoms, and accordingly electron movements during reactions of the substrate and intermediate species at the active site of a $[PMo_{12}O_{40}]^{3-}$ ion. It is a more appropriate property to express changes in catalytic activity in these predominately ionic compounds than, for example, electronegativity, which is more applicable to molecular species. For the cation radii, crystal radii for 6-coordination were employed in this study (36). As noted above, the maximum conversion and selectivity appear to peak at the K^+ salt. This may be deceptive, however, despite the fact that all the compounds are isostructural. The three insoluble alkali metal salts with K^+, Rb^+, and Cs^+ cations were ion exchanged with their respective cations to remove as much adventitious H^+ in their structures as possible. It has been established that when prepared by the synthetic approaches generally employed, some H^+ is always incorporated into the structures of $[PMo_{12}O_{40}]^{3-}$ salts (24). In general, a single ion exchange will remove much of the H^+ (24), although this is only possible for insoluble materials and hence not for the Li^+ and Na^+ salts. Thus, the insoluble K^+, Rb^+, and Cs^+ salts may have been less active in the oxidative hydrogenation of isobutyraldehyde than expected, as the presence of H^+ has a marked enhancing effect on the catalytic abilities of these salts. This is investigated and discussed in more detail below.

TABLE 2

Catalytic Oxidative Dehydrogenation of Isobutyraldehyde Using Salts of Composition $(C^+)_3[PMo_{12}O_{40}]$ (Where $C^+ = H^+$, Li^+, Na^+, K^+, Rb^+, and Cs^+) and the Mixed Cs^+–H^+ Species, $(Cs_nH_{3-n})[PMo_{12}O_{40}]$ (Where $n = 1$, 2, and 2.5)

Catalyst[a]	Temp. (°C)	% Conv.	Rate (10^4 mol min^{-1} g^{-1})	% Selectivity[b] MAL	MAA	ACE	CO	CO_2
$H_3[PMo_{12}O_{40}]$	275	87	1.54	51	4	3	27	15
	300	94	1.66	44	7	3	32	14
$Li_3[PMo_{12}O_{40}]$	275	38	0.67	39	—	9	40	13
	300	71	1.25	59	1	3	21	16
$Na_3[PMo_{12}O_{40}]$	275	31	0.55	55	—	8	27	10
	300	87	1.54	65	2	6	19	9
$K_3[PMo_{12}O_{40}]$	275	48	0.85	34	—	5	37	24
	300	93	1.64	43	2	7	25	23
$Rb_3[PMo_{12}O_{40}]$	275	46	0.81	33	—	17	29	21
	300	74	1.31	46	1	12	22	19
$Cs_3[PMo_{12}O_{40}]$	275	67	1.18	46	2	23	16	14
	300	67	1.18	55	2	13	15	15
$(Cs_{2.5}H_{0.5})[PMo_{12}O_{40}]$	275	98	1.73	50	17	3	19	12
	300	99	1.75	34	27	2	23	13
$(Cs_2H)[PMo_{12}O_{40}]$	275	22	0.39	56	—	10	21	13
	300	46	0.81	54	2	7	22	15
$(CsH_2)[PMo_{12}O_{40}]$	275	26	0.46	58	—	9	20	13
	300	60	1.06	62	1	5	20	12

[a] Mass of catalyst, 0.35 g; W/F = 0.14 g s ml^{-1}.
[b] As in Table 1.

The amount of H^+ present in each of the two soluble catalysts, $Li_3[PMo_{12}O_{40}]$ and $Na_3[PMo_{12}O_{40}]$, was determined using a spectrophotometric method based on the conversion of the base form of the indicator bromothymol blue to its acid form in anhydrous DMF. These studies showed that the Li^+ and Na^+ salts had similar amounts of H^+ present (8 and 5% hydrolysis during preparation, respectively), which is not surprising given their similar synthetic approaches. Thus, the reactivity enhancement afforded by H^+ would be similar and have little effect on their actual relative reactivities. The differences in the catalytic abilities of the K^+, Rb^+, and Cs^+ salts may simply reflect the ease by which these insoluble salts are able to undergo cation-exchange reactions (with $Cs^+ \sim Rb^+ \gg K^+$) and are thus able to replace H^+ by the respective alkali metal cation in the structures of these salts. A reduced presence of H^+ in the insoluble catalysts, particularly Rb^+ and Cs^+, was evident from the Hammett indicator tests using 4-(phenylazo)diphenylamine and dicinnamalacetone, which exhibited a reduced presence of the acid form on the surfaces of these insoluble catalysts compared to that of the soluble catalysts.

As surface area has been shown not to be an important factor in the relative catalytic activities of these species, it would seem that the reason for the observed variations in catalytic activity of these isostructural alkali metal salts may be attributed to the changes in the polarizing ability (as given by ionic potential) of the cation, together with a consideration of the presence of any residual H^+. Catalytic activity would therefore appear to be favoured by low ionic potential, with Cs^+ therefore likely to produce the most active solid catalyst. The order observed is, however, also dependent on the extent of substitution of H^+ for the alkali metal cation in the solid-state structure of the catalyst. However, changes in ionic potential do not actually vary greatly down the alkali metal series (Table 3), especially for the heavier cations, and thus discernable effects on the catalytic activity from these species, especially in the presence of varying amounts of H^+, are difficult to establish. More significant variations would be expected among a series of compounds involving greater changes in the formal oxidation state and hence ionic radius of the cation, as well being provided by variations in the size and distribution of the atoms in a polynuclear cation, such as in the NH_4^+ and Me_4N^+ ions.

To examine a greater range of ionic potential values, a series of compounds with increasing cationic charge and decreasing crystal radius were prepared for comparison with the salt $Cs_3[PMo_{12}O_{40}]$, such that all cations were isoelectronic. These included $Ba_3[PMo_{12}O_{40}]_2$, $La[PMo_{12}O_{40}]$, and $Ce_3[PMo_{12}O_{40}]_4$, which have as their cations Ba^{2+}, La^{3+}, and Ce^{4+}. In this series the polarizing ability of the cation increases greatly, with charge/crystal radius values of 1.34, 2.56, and 3.96, respectively (Cs^+ salt, $Z/r = 0.55$). The catalysis data are given in Table 4. If the polarizing ability of the countercation (as given by ionic potential) is important in the catalytic performance of salts of the $[PMo_{12}O_{40}]^{3-}$ ion, then any effects should be reflected in trends in the rates of reaction and in the conversion percentage of isobutyraldehyde and in the selectivities for the various products. The trends in the rates and conversion percentages at both temperatures suggest an overall decrease with increasing ionic potential, while the trends for the selectivities indicate little effect on the selectivity for methacrolein, except for the Ce^{4+} salt. In general, the rates and conversion percentage to methacrolein are reduced compared to those of $Cs_3[PMo_{12}O_{40}]$, although the latter compound has been ion-exchanged with CsCl to remove as much H^+ as possible. This is, however, impossible for the salts of the Ba^{2+}, La^{3+}, and Ce^{4+} ions as these three compounds are water soluble. Moreover, the actual structures of these salts have not been established, so that the arrangement of the cations around the $[PMo_{12}O_{40}]^{3-}$ ion in the solid-state structures of these compounds are currently unknown, and this may be of particular importance in the actual processes that occur at the catalyst surface. It should also be noted that there is some evidence, for the alkaline earth metal cations, that the $[PMo_{12}O_{40}]^{3-}$ salts are difficult to synthesize (37, 38). It may be that, like the Li^+ and Na^+ salts, these salts (specifically Ba^{2+} in the present case) form only upon calcination at higher temperatures. Indeed, the XRD patterns of these species undergo significant changes upon calcination and are currently under investigation.

The increased selectivities to methacrolein and methacrylic acid in the case of $Ce_3[PMo_{12}O_{40}]_4$ appear contrary to the observed trend in catalytic behaviour of the Cs^+-, Ba^{2+}-, and La^{3+}-containing compounds. However, it should be noted that of all the countercations discussed above, only Ce(IV) is potentially capable of undergoing changes in the oxidation state under the conditions employed in the catalysis. Recently, it has been shown that for the mixed metal

TABLE 3

Crystallographic, Thermogravimetric Analysis, and Surface Area Data for the Alkali Metal and NH_4^+ Salts, $(C^+)_3[PMo_{12}O_{40}]$ (where $C^+ = Li^+, Na^+, K^+, Rb^+, Cs^+$, and NH_4^+)

Salt	Cation crystal radius (Å)[a]	Ionic potential[b]	Unit cell dimension (Å)	% H_2O loss at 300°C	Surface area ($m^2\ g^{-1}$)
$Li_3[PMo_{12}O_{40}]$	0.90	1.11	11.734(2)	11.0	4.8
$Na_3[PMo_{12}O_{40}]$	1.16	0.86	11.936(1)	3.5	3.2
$K_3[PMo_{12}O_{40}]$	1.52	0.66	11.5975(2)	5.2	109
$Rb_3[PMo_{12}O_{40}]$	1.66	0.60	11.6687(5)	3.3	94
$Cs_3[PMo_{12}O_{40}]$	1.81	0.55	11.8412(9)	1.9	117
$(NH_4)_3[PMo_{12}O_{40}]$	—	—	11.6575(3)	3.7	120

[a] Six coordination.

[b] Ionic potential is given by the charge/crystal radius.

TABLE 4

Catalytic Oxidative Dehydrogenation of Isobutyraldehyde Using Salts of Composition $(C^{n+})_{3/n}[PMo_{12}O_{40}]$ (Where $C^+ = Cs^+$, Ba^{2+}, La^{3+}, Ce^{4+}, NH_4^+, and Me_4N^+)

Catalyst[a]	Temp. (°C)	% Conv.	Rate (10^4 mol min^{-1} g^{-1})	% Selectivity[c] MAL	MAA	ACE	CO	CO_2
$Cs_3[PMo_{12}O_{40}]$	275	67	1.18	46	2	23	16	14
	300	67	1.18	55	2	13	15	15
$Ba_3[PMo_{12}O_{40}]_2$	275	28	0.49	15	—	17	55	13
	300	34	0.60	46	—	8	33	13
$La[PMo_{12}O_{40}]$	275	23	0.41	51	—	9	34	7
	300	40	0.70	48	1	7	32	13
$Ce_3[PMo_{12}O_{40}]_4$	275	32	0.56	74	—	16	2	8
	300	22	0.39	80	—	11	2	8
$(NH_4)_3[PMo_{12}O_{40}]$[b]	275	61	1.88	71	<1	6	10	12
	300	81	2.50	62	2	5	18	13
$(Me_4N)_3[PMo_{12}O_{40}]$[b]	275	95	2.93	74	2	2	13	9
	300	99	3.06	50	10	1	23	16

[a] Mass of catalyst, 0.35 g; W/F = 0.14 g s ml^{-1}.
[b] Mass of catalyst, 0.20 g; W/F = 0.08 g s ml^{-1}.
[c] As in Table 1.

species $H_4[PMo_{11}VO_{40}]$ under the conditions of catalysis, the vanadium leaves the polyoxomolybdate framework and results in V(IV) counterions of a partially reduced polyoxomolybdophosphate ion (22). Indeed, the vanadyl salt of $[PMo_{12}O_{40}]^{3-}$, i.e., $H(VO)[PMo_{12}O_{40}]$, exhibits reactivity similar to that of the original mixed metal catalyst (22).

A second way of changing the ionic potential of a cation is by delocalizing the charge over several atoms through the use of a polynuclear cation. For this purpose catalysis data for salts of the $[PMo_{12}O_{40}]^{3-}$ ion containing the NH_4^+ and $(CH_3)_4N^+$ cations may be compared with the data for $Cs_3[PMo_{12}O_{40}]$. The data are also given in Table 4. Although there are some differences in the sizes of these ions, the main variations concern the locations and magnitudes of the (net) atomic charges of the atoms that constitute these cations. The net atomic charges for the atoms of the NH_4^+ and $(CH_3)_4N^+$ ions, based on extended-Hückel molecular orbital calculations, are NH_4^+ (N, +0.15, and H, +0.21) and $(CH_3)_4N^+$ (C, +0.13; N, +0.14, and H, +0.03). As the ionic potential is decreased or, as in the case of NH_4^+ and $(CH_3)_4N^+$, a progressively decreasing concentration of charge at any one atom based on the net charges of the atoms concerned, the conversion percentage increased, while the selectivity to methacrolein and methacrylic acid both increased slightly compared to that of $Cs_3[PMo_{12}O_{40}]$. The trends observed in the catalytic performance of the above salts support the proposal of the effect of ionic potential of the cation affecting the electron distribution of the transition states and/or intermediates in the oxidative dehydrogenation of isobutyraldehyde. Further increases in size of the cation, such as those found in the series Et_4N^+, Pr_4N^+, and $^nBu_4N^+$, do not result in greater increases in conversion percentage, as the charge on the atoms does not vary greatly with increasing size of the alkyl group (32).

D. *Effect of Added H^+ on the Catalytic Ability of the $(Cs_nH_{3-n})[PMo_{12}O_{40}]$ Salts*

(i) Catalysis studies. To examine the effect of the presence of added H^+ on catalytic ability, a series of materials with varying amounts of H^+ in their structures were synthesized, with Cs^+ as the alkali metal cation. The series chosen was $(Cs_nH_{3-n})[PMo_{12}O_{40}]$, where n had nominal values of 1, 2, and 2.5. These were examined for catalytic activity compared to that of $Cs_3[PMo_{12}O_{40}]$ ($n = 3$) and also the free acid, $H_3[PMo_{12}O_{40}]$ ($n = 0$), with the data given in Table 2. The effect of the presence of some H^+ in the structure on the oxidative dehydrogenation reaction is evident, although the addition of greater amounts of H^+ appears detrimental to the reaction. Thus, the maximum conversion and selectivity to methacrolein and methacrylic acid were achieved with the compound $Cs_{2.5}H_{0.5}[PMo_{12}O_{40}]$.

(ii) X-ray diffraction studies. Examination of the XRD patterns of the compounds $(Cs_nH_{3-n})[PMo_{12}O_{40}]$, where $n = 0$, 1, 2, 2.5, and 3, showed that when isolated directly from solution, there was no evidence for the presence of two phases for $n = 2.5$ and 2, but for $n = 1$ the XRD patterns of both $Cs_3[PMo_{12}O_{40}]$ and $H_3[PMo_{12}O_{40}]$ (probably as the 23- or lower hydrate) were present. Thus, for $n \geq \sim 2$, the two cations appear to form a single mixed phase when precipitated from solution, which allows for some variability in composition. Upon heating to 300°C for 4 h, it was hard

to establish the presence of the anhydrous $H_3[PMo_{12}O_{40}]$ phase in $(CsH_2)[PMo_{12}O_{40}]$ as the diffraction pattern of the dehydrated acid was not well defined.

(iii) ^{31}P solid state NMR studies. To further explore the possibility of the formation of a solid solution for $(Cs_nH_{3-n})[PMo_{12}O_{40}]$ with $n=2$ and 2.5, the solid state ^{31}P NMR of all compounds in the series ($n=0$, 1, 2, 2.5, and 3) were obtained, both on freshly isolated material and after heating to 300°C for 4 h. The spectra of the calcined materials are given in Fig. 4, along with those of $H_3[PMo_{12}O_{40}]\cdot 23H_2O$ and partially rehydrated $H_3[PMo_{12}O_{40}]$ following thermal treatment.

When freshly precipitated, the samples with $n=2.5$ and 2 showed no evidence of two signals, and both had a chemical shift almost the same as that of $Cs_3[PMo_{12}O_{40}]$. This appeared at -4.55 ± 0.03 ppm in all of the spectra, whether the samples were calcined or not. Only with $n=1$ was evidence for two signals apparent (at -4.18 and ~ -4.5 ppm). In this case two components could be observed, which is consistent with the XRD data described above, showing the presence of a second phase at this composition. In view

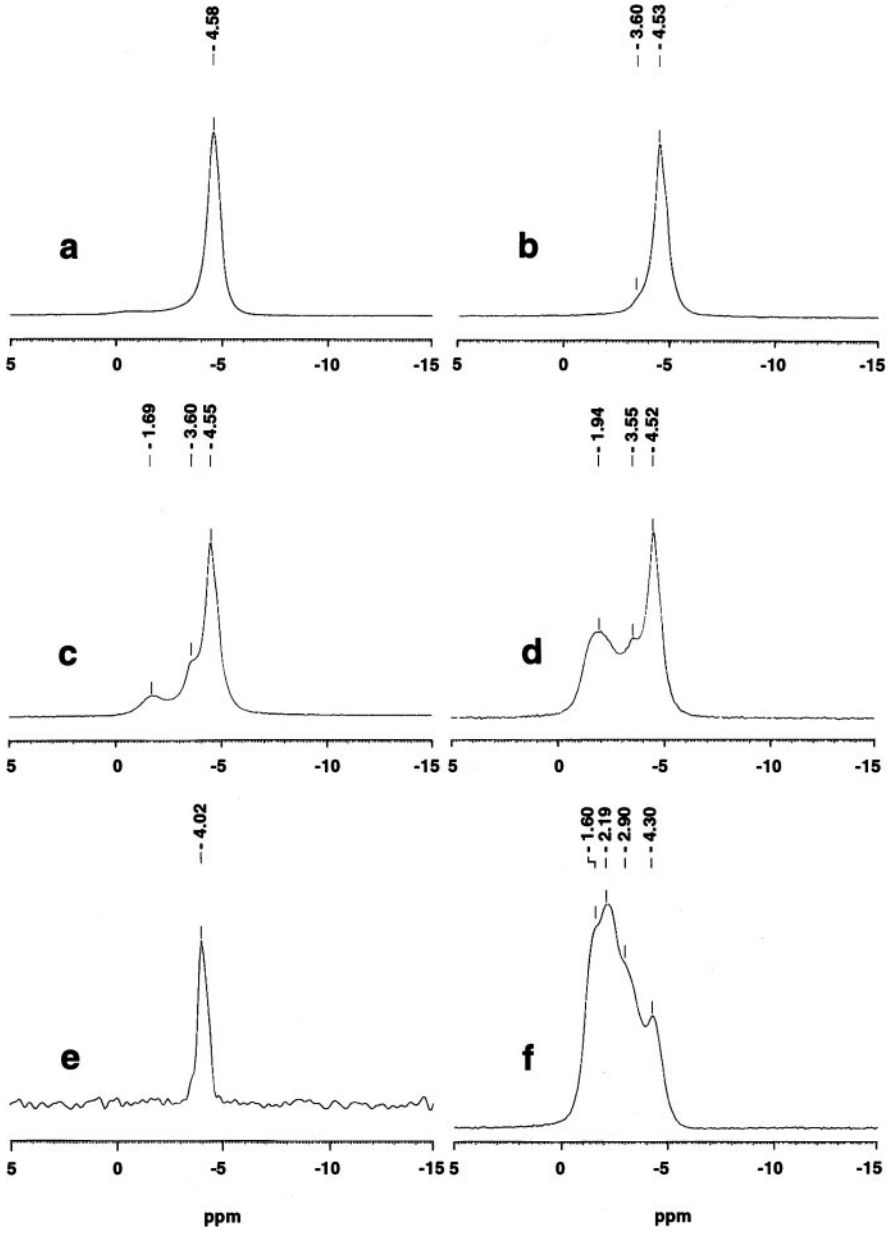

FIG. 4. Solid-state ^{31}P NMR spectra of $Cs_nH_{3-n}[PMo_{12}O_{40}]$ ($n=0$, 1, 2, 2.5, and 3): (a) $Cs_3[PMo_{12}O_{40}]$, (b) $Cs_{2.5}H_{0.5}[PMo_{12}O_{40}]$, (c) $Cs_2H[PMo_{12}O_{40}]$, and (d) $CsH_2[PMo_{12}O_{40}]$, all calcined at 300°C for 4 h, (e) $H_3[PMo_{12}O_{40}]\cdot 23H_2O$, and (f) $H_3[PMo_{12}O_{40}]$ that has been partially rehydrated after thermal treatment at 300°C.

of the closeness of the chemical shifts of $Cs_3[PMo_{12}O_{40}]$ and $H_3[PMo_{12}O_{40}] \cdot 23H_2O$ (−4.02 ppm, Fig. 4e) it is difficult to separate the individual signals for $n = 2.5$ and 2, and solid solutions may even form for these compositions. This appears to be slightly different from the results previously obtained by Black *et al.* (39) on the analogous $K_nH_{3-n}[PMo_{12}O_{40}]$ system, where separate peaks associated with $K_3[PMo_{12}O_{40}]$ and partially hydrated $H_3[PMo_{12}O_{40}]$ were able to be resolved. This may, however, depend on the extent of hydration of the free acid, which varies over a range of chemical shifts [Fig. 4f and Ref. (39)].

Upon heating the materials of composition $Cs_nH_{3-n}[PMo_{12}O_{40}]$ to 300°C for 4 h, significant changes to the spectra were observed. The presence of $Cs_3[PMo_{12}O_{40}]$ (Fig. 4a) was evident in all of the spectra, indicating the stability of this phase, but broad peaks at −3.55 and ∼−1.8 ppm developed for $n = 2.5$, 2, and 1 (Figs. 4b–4d, respectively). These broad peaks are consistent with the formation of partially hydrated forms of $H_3[PMo_{12}O_{40}]$ (Fig. 4f). Somewhat similar results were observed for both the $K_nH_{3-n}[PMo_{12}O_{40}]$ (39) and $Cs_nH_{3-n}[PW_{12}O_{40}]$ systems (40). In the former the appearance of several peaks was interpreted in terms of the growth of an epitaxial surface layer of essentially dehydrated acid on $K_3[PMo_{12}O_{40}]$. However, in the latter the presence of separate components was suggested, with the partially dehydrated acid, $H_3[PW_{12}O_{40}]$, trapped in the $Cs_3[PW_{12}O_{40}]$ structure. More recently, examination of the $Cs_nH_{3-n}[PMo_{12}O_{40}]$ system ($0 < n < 3$) following calcination at 350°C using XRD, Raman spectroscopy, and XPS for surface chemical analysis has concluded that two phases ($Cs_3[PMo_{12}O_{40}]$ and $H_3[PMo_{12}O_{40}]$) exist at all compositions, with the hydrated acid phase coating the pure cesium salt (41). The solid-state ^{31}P NMR data obtained in the present study are consistent with this latter suggestion.

II. The Mechanism of the Oxidative Dehydrogenation of Isobutyraldehyde over Salts of the $[PMo_{12}O_{40}]^{3-}$ Ion

A. Mechanism of Oxidative Dehydrogenation of Isobutyraldehyde

Reaction of isobutyraldehyde in the presence of oxygen over salts of the $[PMo_{12}O_{40}]^{3-}$ ion at temperatures from 275 to 350°C produced methacrolein, methacrylic acid, acetone, CO, and CO_2 as the major products observed. In the present studies there was no evidence for the formation of isobutyric acid, propene, or acetic acid, although the last has been observed as a very minor product in a previous study using $H_5V_2Mo_{10}O_{40}$ as the catalyst (42). The methacrylic acid was only formed when the conversion of the isobutyraldehyde was greater than about 50%. Although isobutyraldehyde can be oxidised to isobutyric acid fairly readily, it appears that under the conditions employed in the present studies this reaction does not proceed to any great extent at the contact times used, as methacrylic acid would have been observed even at low isobutyraldehyde conversions if this reaction had occurred. Moreover, no isobutyric acid was directly observed as a product species. Examination of the data in Figs. 1 and 2 and in Tables 2 and 4 also indicates that the formation of acetone is favoured at lower temperatures (275 vs 300°C) and that the presence of H^+ favours the formation of CO as well as reduction of acetone formation.

The mechanism of formation of the above products can be accounted for on the basis of Scheme 1:

$$(CH_3)_2CHCHO_{(gas)} \rightarrow [(CH_3)_2CHCHO]_{ads} \quad [2]$$

$$[(CH_3)_2CHCHO]_{ads} \xrightarrow{[O]} H_2C{=}C(CH_3)CHO + H_2O \quad [3]$$

$$[H_2C{=}C(CH_3)CHO]_{ads} \xrightarrow{2[O]} (CH_3)_2CO + H_2O + CO \quad [4]$$

$$[(CH_3)_2CHCHO]_{ads} \xrightarrow{n[O]} xCO + yCO_2 + zH_2O \quad [5]$$

SCHEME 1

where [O] represents a lattice oxygen. The last reaction has not been written stoichiometrically as the relative yields of CO and CO_2 are uncertain and, also, as $[(CH_3)_2CHCHO]_{ads}$ in Eq. [5] can be replaced by adsorbed methacrolein or acetone, the complete oxidation of both of these products may possibly occur prior to their desorption. According to the above scheme, the yield of CO will always be greater than that of acetone (compare Eqs. [4] and [5]), which is the case observed in the present studies. As H^+ favours the formation of CO over acetone, presumably Eq. [5] is also facilitated in some way by the presence of H^+ and likely favours CO over CO_2 as the formation of the latter is little affected by H^+. The above mechanism is only meant to convey a broad, overall approach and not a detailed description of the individual steps involved.

The above reaction scheme is similar to, but simpler than, that of the equivalent oxidative dehydrogenation reaction of isobutyric acid in that it does not require a (significant) competing pathway that is dependent on the presence of H^+, i.e., on the Brønsted acidity of the catalyst (1, 19). In the case of isobutyric acid this pathway involves the breakdown of adsorbed isobutyric acid to give propene, CO, and H_2O. Thus, any trends associated with cation effects (and thus ionic potential) will be more easily seen in the present study as any contributions from this competing reaction do not occur.

The formation of methacrolein from isobutyraldehyde over a $[PMo_{12}O_{40}]^{3-}$-containing catalyst is an oxidative dehydrogenation reaction. Thus, following adsorption of the isobutyraldehyde (Eq. [2] above), the sequential loss of two hydrogen atoms must occur, resulting in methacrolein (these are combined in Eq. [3]). The mechanism of the oxidative dehydrogenation of isobutyric acid to yield methacrylic acid is similar. For the

oxidative dehydrogenation of isobutyric acid three mechanisms have been proposed for the sequential loss of the two hydrogen atoms, involving either heterolytic or homolytic processes (1, 20, 43). Similar mechanisms can be proposed in the present case for the oxidative dehydrogenation of isobutyraldehyde, but whether the intermediate is a carbocation, carbanion, or radical species cannot be inferred without further investigations. However, some proposals concerning the effects of variations in the countercations can be made. Thus, upon adsorption of an isobutyraldehyde molecule, a certain orientation of the molecule on the oxomolybdate surface of the polyanion will occur. In the vicinity of the adsorbed isobutyraldehyde molecule will reside various countercations. Presumably, the ionic potential of these cations (or even single cation) plays a role in the two dehydrogenation steps that lead to methacrolein (Eq. [3] above). It is likely, therefore, that any strong electric field effects, represented by a high ionic potential, are likely to have adverse effects on the movement of electrons and hence bond stretching and breaking in the formation of the transition states. This will, in turn, act to increase one or both of the free energies of activation for loss of the hydrogen (in whatever form) and hence decrease the rate of reaction and thus the extent of conversion (for a given W/F or contact time at a set temperature). Thus, by lowering of the ionic potential or through dissipation of the cationic charge over several atoms, such as with an NH_4^+ or $(CH_3)_4N^+$ ion, the maximum rate of conversion and formation of the desired product can be achieved. Changes in ionic potential might also be expected to influence the selectivities to the various products as these are the result of competing reactions (Eqs. [3]–[5] above). Thus, for the alkali metal, Ba^{2+} and La^{3+} salts, increasing ionic potential appears to disfavour the formation of acetone while having little effect on the selectivity to methacrolein. The NH_4^+ and $(CH_3)_4N^+$ salts behave similarly. The Ce^{4+} salt, however, while exhibiting low conversion as a result of its very high ionic potential, has a very high selectivity to methacrolein. As noted above, this is likely the result of the electron transfer capability of the Ce(IV)/Ce(III) couple, such as has been suggested for V(V)/V(IV) in (thermally rearranged) $H_4[PMo_{11}VO_{40}]$ and in $H(VO)[PMo_{12}O_{40}]$ (22). Notably, in the oxidative dehydrogenation of isobutyric acid, the latter two catalysts exhibit similar conversion percentages to that of $H_3[PMo_{12}O_{40}]$, but have significantly increased selectivities percentage to methacrylic acid as a result of the presence of vanadium (22).

Comparisons with the data obtained above for the alkali metals as countercations can be made with the studies reported by Akimoto *et al.* (1) on the oxidative dehydrogenation of isobutyric acid to yield methacrylic acid, although in this work the catalysts were supported using quartz sand. Interestingly, in these studies, the trend with varying alkali metal cation showed increasing promotion of reaction as the alkali metal cation increased in size, that is, with decreasing polarizing ability, the trend proposed in the present studies. Similarly, the same trend was also observed by Kaszelten and Moffat (13) in their studies of the partial oxidation of methane using N_2O over silica-supported $H_3PMo_{12}O_{40}$ and its salts. Notwithstanding the fact that in both of these studies the catalysts were supported, unlike in the present studies, it is likely that, as similar dependencies on the polarizing ability of the countercation occur in these reactions, the countercations again play an active role in influencing electron movements in the transition state(s) as described above.

In the investigation of the effect of H^+ on the conversion percentages and rates of reaction for the sequence of compounds $(Cs_nH_{3-n})[PMo_{12}O_{40}]$ ($n = 1$, 2, 2.5, and 3) in the present work, the maximum enhancement was observed with $(Cs_{2.5}H_{0.5})[PMo_{12}O_{40}]$. Interestingly, similar maxima in reactivity close to this composition have been observed in other quite unrelated systems, but using acidic salts of $[PW_{12}O_{40}]^{3-}$, such as in the gas-phase methanol dehydration to dimethyl ether at 180°C and *n*-butane isomerization over $(Cs_nH_{3-n})[PW_{12}O_{40}]$ at 200°C (40), which gave the highest activity over the range $n = 2.7$ to 2 for the former and near 2 for the latter, and in the liquid-phase isobutane/2-butene alkylation at 80°C and 2.5 MPa over the acidic Cs^+, NH_4^+, and K^+ salts of $H_3[PW_{12}O_{40}]$ (44), which yielded a maximum of $n = 2.5$ for the NH_4^+ and K^+ salts and a maximum in the range of $2 \leq n \leq 2.5$ for the Cs^+ salt. Correlations with surface acidity have been proposed to explain the results in these studies, and it is apparent that surface acidity is important in the present study as well.

Assuming that the H^+ is evenly distributed throughout the surface and bulk of the catalyst, then the variation of surface acidity with *n* in $(Cs_nH_{3-n})[PMo_{12}O_{40}]$ reaches a maximum value (46 μmol g^{-1}) at $n = 2.5$ in the present studies. The surface acidity, which is proportional to the surface area times $(3-n)$, the actual H^+ content in $(Cs_nH_{3-n})[PMo_{12}O_{40}]$, is highly dependent on surface area and is slightly lower than the analogous value found for the maximum in the related series of compounds $(Cs_nH_{3-n})[PW_{12}O_{40}]$ (~70 μmol g^{-1}) (45, 46). This is a direct consequence of the smaller surface area of $(Cs_{2.5}H_{0.5})[PMo_{12}O_{40}]$ (77 $m^2 g^{-1}$) compared to that of $(Cs_{2.5}H_{0.5})[PW_{12}O_{40}]$ (~130 $m^2 g^{-1}$). Thus, although a catalytic reaction may occur by bulk catalysis-type II, as in the present case, if the kinetically accessible mechanism contains a step that depends on H^+, then variations in rate will actually depend on surface area in an indirect way through the changing surface acidity. This is most obvious when there are large changes in surface area, as occurs with these types of compounds, i.e., the series $(Cs_nH_{3-n})[PMo_{12}O_{40}]$ in the present case, which shows a large increase in surface area for compositions above $n = 2$. Thus, for the series

$(Cs_nH_{3-n})[PMo_{12}O_{40}]$, where $n = 0$, 1, 2, 2.5, and 3, the surface areas were 1.2, 0.8, 2.9, 77, and 117 $m^2 g^{-1}$, respectively.

B. The Site of Anionic (Lattice) Oxygen Involved in the Oxidative Dehydrogenation of Isobutyraldehyde (and Related) Substrates

The mechanism represented by Eqs. [2]–[5] above describes a series of steps in the oxidative dehydrogenation of isobutyraldehyde and concentrates on the fate of the organic substrate. However, it has been established in previous studies that the source of oxygen, i.e., [O] in Eqs. [3]–[5], is actually from the polyoxomolybdate framework, which is eventually replenished by the molecular dioxygen in the catalysis input stream. Infrared studies have suggested that it is the bridging oxygen atoms of the $[PMo_{12}O_{40}]^{3-}$ ion that supply the oxygen for this process (47–51). Thus, reduction of, for example, $H_3PMo_{12}O_{40}$ by H_2 at 280–320°C showed that the ν(Mo–O–Mo) bands decreased relative to the ν(Mo=O) band, suggesting loss of bridging oxygen atoms. Notably, the ν(P–O) band also decreased in intensity during this reduction process. However, it has been shown that similar reductions in relative intensity for these same bands also occur as a result of electrochemical reduction, where no structural changes take place.

Examination of the Mulliken population analyses obtained from extended-Hückel calculations of the bonds from molybdenum to the four types of oxygen atoms (a measure of bond order) are given in Table 5. These values reflect the corresponding bond distances, which are also included in the table. It is apparent that of the different types of oxygen atoms, with the exception of the inner oxygen atom, a bridging oxygen atom within an Mo_3O_{13} subunit is the likely candidate for the source of the lattice oxygen. This can be confirmed by calculating the change in total stabilization energy ΔE_T (where E_T for a particular species is the sum of the one-electron energies as calculated using the extended-Hückel molecular orbital method) for each of the potential oxygen positions ($O_a \rightarrow O_d$) for the reaction

$$[PMo_{12}O_{40}]^{3-} \rightarrow [PMo_{12}O_{39}]^{3-} + [O]. \qquad [6]$$

This reaction simply represents loss of an oxygen atom (a lattice oxygen) from the polyoxomolybdate framework and involves the formation of Mo(V) [two Mo(V) for every phosphopolyoxomolybdate unit]. The change in total stabilization energies, ΔE_T (eV), for this reaction increases in the order

$$O_a(+7.64) < O_b(+12.47) < O_d(+12.87) < O_c(+12.97).$$

Not surprisingly, the lowest energy requirement is that for an inner oxygen (O_a). However, this is inaccessable and will not be involved in the catalysis process. The next most favorable site is that of an oxygen atom linking molybdenum atoms within a Mo_3O_{13} subunit (O_b), followed by a terminal oxygen atom (O_d) and finally a bridging oxygen atom between Mo_3O_{13} subunits (O_c). Although the latter three possibilities are quite similar in their energy requirements, that of loss of an oxygen atom within a Mo_3O_{13} subunit is slightly favoured. Thus, the above calculations support loss of a bridging oxygen atom during oxidative dehydrogenation (and also oxidation) reactions over a $[PMo_{12}O_{40}]^{3-}$-containing catalyst, with an oxygen atom within a Mo_3O_{13} subunit likely providing the source of oxygen.

TABLE 5

Mulliken Population Analysis for the $[PMo_{12}O_{40}]^{3-}$ Ion

Bond	Bond distance (Å)	Population analysis
P–O	1.542	0.688
Mo–O_a (inner)	2.434	0.128
O_b (bridging O within an Mo_3O_{13} unit)	1.923	0.442
O_c (bridging O between Mo_3O_{13} units)	1.911	0.475
O_d (terminal)	1.676	0.726

C. The Role of H^+ and the Mechanism of Oxidative Dehydrogenation of Isobutyraldehyde

It is evident that the presence of H^+ has a marked effect in the catalytic ability of the $[PMo_{12}O_{40}]^{3-}$ ion. The presence of H^+ could potentially affect the mechanism given by Eqs. [2] to [5] in several ways and may involve either protonation of the $[PMo_{12}O_{40}]^{3-}$ ion or protonation of the substrate (isobutyraldehyde), the latter probably as part of a transition state or intermediate.

The likely protonation sites on the $[PMo_{12}O_{40}]^{3-}$ ion were investigated using extended-Hückel molecular orbital calculations, to see the effect of protonation on the HOMO–LUMO gap and the total stabilization energy of the system. Protonation may decrease the HOMO–LUMO energy gap, therefore making it easier to reduce this anion, which occurs during catalysis (1).

Placing a single H around the $[PMo_{12}O_{40}]^{3-}$ ion (H^+ plus $[PMo_{12}O_{40}]^{3-}$, to give an overall $[HPMo_{12}O_{40}]^{2-}$ moiety) in tetrahedral geometries with O–H distances as short as 1.00 Å, the approximate O–H distance in water, for each of the oxygen environments (with the exception of O_a, which is an internal atom) showed no effect on the HOMO–LUMO gap. An alternative approach to protonation would be to delocalize the interaction over several sites, by locating the H between several oxygen atoms, so that it forms weak hydrogen bonds with these oxygen atoms. The effect of protonation of the $[PMo_{12}O_{40}]^{3-}$ ion on the HOMO–LUMO gap was therefore examined by allowing a hydrogen to approach the anion along selected directions, such that the hydrogen would interact with several oxygen atoms

in different environments. Three cases were investigated, which included approaches along a C_3 axis of the anion from opposite sides, such that (i) the hydrogen interacted equally with three bridging oxygen atoms (O_b) within a single Mo_3O_{13} unit or (ii) with three bridging oxygen atoms (O_c) linking three Mo_3O_{13} units and (iii) along the C_2 axis of the anion, such that interactions occurred with two O_b and two O_c oxygen atoms. In the first and third approaches, interaction was also possible with an internal oxygen atom O_a.

While protonation yielded an increase in the total stabilization energies, resulting in energy "minima" along all three pathways, only the third direction of approach actually showed a decrease in the HOMO–LUMO gap. This occurred at a P–H distance of ~2.3 Å, which is slightly inside the confines of the peripheral oxygen atoms of the anion. This decrease was only some 0.19 eV in a HOMO–LUMO gap of 4.79 eV, which is not highly significant, even considering the approximations in the extended-Hückel MO calculational methodology. Thus, it would seem unlikely that protonation is important in increasing the ease of reduction of the anion in the catalytic process. In passing, however, it may be noted that, in protic solvents, protonation does occur following multiple reductions of the $[PMo_{12}O_{40}]^{3-}$ ion (6), as a way of reducing (and hence stabilizing) the increasing anionic charge.

An alternative possibility may be protonation of the isobutyraldehyde, either as part of a transition state and/or intermediate. This would occur at an electron-rich atom of the isobutyraldehyde molecule, probably the carbonyl oxygen atom. In doing so, this would help to delocalize the negative charge of a possible carbanion intermediate, but not a carbocation, and less likely, a radical intermediate. Thus, the observed enhancement of catalytic activity in the presence of H^+ may provide evidence for the formation of a carbanion intermediate and the mechanism of Otake and Onoda (43). Protonation of the organic substrate is also supported by the recent studies of Langepape *et al.* (41), who have shown that, in the $Cs_nH_{3-n}[PMo_{12}O_{40}]$ system ($0 < n < 3$), $H_3[PMo_{12}O_{40}]$ coats the $Cs_3[PMo_{12}O_{40}]$. Thus, as the oxidative dehydrogenation of isobutyraldehyde occurs by bulk catalysis-type II, with the organic substrate adsorbing on the catalyst surface, the presence of H^+ on this surface and thus available for protonation of the substrate supports this possible pathway. Currently, however, it is not possible to differentiate between protonation of the anion (following reduction) or the substrate (transition state or intermediate stages) and both may play a role in the mechanism of oxidative dehydrogenation over a polyoxometalate catalyst, although the latter appears the most likely at the present time.

Kaszelten and Moffat (10–13) have also provided evidence for the involvement of protons in the partial oxidation of methane using N_2O over silica-supported $H_3PMo_{12}O_{40}$ and its salts. It was proposed that in this case oxygen vacancies could be formed by a dehydration mechanism, through the elimination of a water molecule from two protonated $[PMo_{12}O_{40}]^{3-}$ ions, yielding one intact anion and the second containing a vacancy. The vacancy could then be involved in further processes, such as supplying a favorable adsorption site or as a site that might receive an oxygen atom following gas-phase dissociation of the oxidant. This reaction was studied at 500–590°C, which is above the temperature of decomposition of $H_3PMo_{12}O_{40}$ by loss of constitutional water (~400°C). However, under the conditions of reaction of the supported catalyst Kaszelten and Moffat were able to show that not all of the $[PMo_{12}O_{40}]^{3-}$ ions had decomposed. It thus appears that oxidation catalysts based on $[PMo_{12}O_{40}]^{3-}$ (and thus also likely $[PW_{12}O_{40}]^{3-}$) may exhibit different types of mechanisms over different temperature regimes.

ACKNOWLEDGMENTS

The authors would like to acknowledge Mr. M. Littlefair, Ms. J. Ewing, and Ms. S. Bell of B.H.P. (Newcastle Laboratories) for performing the surface area and pore volume and size measurements, Ms. C. Allen and Mr. K. Grice for help in obtaining the structural data, and Mr. G. Weber and Mr. D. Phelan, of the University Microscopy Unit, for recording the scanning electron microscopy images. Dr. J. Hu would also like to acknowledge the University of Newcastle for the award of a UNRS and an OPRS.

REFERENCES

1. Akimoto, M., Tsuchida, Y., Sato, K., and Echigoya, E., *J. Catal.* **72**, 83 (1981).
2. Konishi, Y., Sakata, K., Misono, M., and Yoneda, Y., *J. Catal.* **77**, 169 (1982).
3. Misono, M., *in* "Polyoxometalates: From Platonic Solids to Anti-Retroviral Activity" (M. T. Pope and A. Müller, Eds.), p. 255. Kluwer, Dordrecht, 1994.
4. Misono, M., *Catal. Rev.-Sci. Eng.* **29**, 269 (1987); **30**, 339 (1988).
5. Mizuno, N., and Misono, M., *Chem. Rev.* **98**, 199 (1998).
6. Pope, M. T., "Heteropoly and Isopoly Oxometalates." Springer-Verlag, Berlin, 1983.
7. Hu, J., Burns, R. C., and Guerbois, J.-P., *J. Mol. Catal. A: Chem.* **152**, 141 (2000).
8. Cavani, F., Etienne, E., Favaro, M., Galli, A., Trifirò, F., and Hecquet, G., *Catal. Lett.* **32**, 215 (1995).
9. Cavani, F., Comuzzi, C., Dolcetti, G., Finke, R. G., Lucchi, A., Trifirò, F., and Trovarelli, A., *in* "Heterogeneous Hydrocarbon Oxidation" (B. K. Warren and S. T. Oyama, Eds.), ACS Symposium Series 638, Chap. 10, p. 140. *Am. Chem. Soc.*, Washington, DC, 1996.
10. Kaszelten, S., and Moffat, J. B., *J. Catal.* **106**, 512 (1987).
11. Kaszelten, S., and Moffat, J. B., *J. Catal.* **109**, 206 (1988).
12. Kaszelten, S., and Moffat, J. B., *J. Catal.* **112**, 54 (1988).
13. Kaszelten, S., and Moffat, J. B., *J. Catal.* **116**, 82 (1989).
14. Muneyama, E., Kunishige, A., Ohdan, K., and Ai, M., *J. Mol. Catal.* **89**, 371 (1994).
15. Ishimi, K. (Nippon Kayaku Co. Ltd.) *Japan Kokai*, 54,046,705 (1975).
16. Ando, N. (Japan Synthetic Rubber Co. Ltd.) *Japan Kokai*, 53,124,211 (1978).
17. Wu, T., Leng, Y., Yang, H., Wang, G., Zhang, H., Hua, S., Jiang, Y., and Zhen, K., *J. Mol. Catal.* **57**, 193 (1989).

18. Wang G., Hu, J., Yang, H., and Wu, T., *Gaodeng Xuexiao Huaxue Xuebao* (Chemical Journal of Chinese Universities) **11**, 1249 (1990).
19. Akimoto, M., Shima, K., Ikeda, H., and Echigoya, E., *J. Catal.* **86**, 173 (1984).
20. McGarvey, G. B., and Moffat, J. B., *J. Catal.* **132**, 100 (1991).
21. Komaya, T., and Misono, M., *Chem. Lett.* 1177 (1983).
22. Cadot, E., Marchal, C., Fournier, M., Tézé, A., and Hervé, G., *in* "Polyoxometalates: From Platonic Solids to Anti-Retroviral Activity" (M. T. Pope and A. Müller, Eds.), p. 135. Kluwer, Dordrecht, 1994.
23. Tsigdinos, G. A., Ph.D. thesis, Boston University, 1961.
24. McGarvey, G. B., and Moffat, J. B., *J. Catal.* **128**, 69 (1991).
25. Massart, R., Contant, R., Fruchart, J. M., Ciabrini, M., and Fournier, M., *Inorg. Chem.* **16**, 2916 (1977).
26. Kozhevnikov, I. V., *Russ. Chem. Rev.* **56**, 811 (1987).
27. Clare, B. W., Cook, D., Ko, E. F. C., Mac, Y. C., and Parker, A. J., *J. Am. Chem. Soc.* **88**, 1911 (1966).
28. Benesi, H. A., and Winquist, B. H. C., *Adv. Catal.* **27**, 97 (1978).
29. Mealli, C., and Proserpio, D. M., *J. Chem. Educ.* **67**, 399 (1990).
30. Strandberg, R., *Acta Chem. Scand. A* **29**, 359 (1975).
31. Allmann, R., *Acta Chem. Scand. A* **30**, 152 (1976).
32. Young, B., M. Sci. Studies Thesis, University of Newcastle, 1998.
33. Highfield, J. G., and Moffat, J. B., *J. Catal.* **88**, 177 (1984).
34. McMonagle, J. B., and Moffat, J. B., *J. Colloid Interface Sci.* **101**, 479 (1984).
35. Boeyens, J. C. A., McDougal, J., and Smit, J. V. R., *J. Solid State Chem.* **18**, 191 (1976).
36. Shannon, R. D., *Acta Crystallogr. A* **32**, 751 (1976).
37. McGarvey, G. B., and Moffat, J. B., *Catal. Lett.* **16**, 173 (1992).
38. McGarvey, G. B., Taylor, N. J., and Moffat, J. B., *J. Mol. Catal.* **80**, 59 (1993).
39. Black, J. B., Clayden, N. J., Gai, P. L., Scott, J. D., Serwicka, E. M., and Goodenough, J. B., *J. Catal.* **106**, 1 (1987).
40. Essayem, N., Coudurier, G., Fournier, M., and Védrine, J. C., *Catal. Lett.* **34**, 223 (1995).
41. Langpape, M., Millet, J. M. M., Ozkan, U. S., and Boudeulle, M., *J. Catal.* **181**, 80 (1999).
42. Müller, E., and Hofmann, H., *Chem. Eng. Sci.* **42**, 1705 (1987).
43. Otake, M., and Onoda, T., *in* "Proceedings, 7th International Congress on Catalysis, Tokyo, 1980" (T. Seiyama and K. Tanabe, Eds.), B3. Elsevier, Amsterdam, 1981.
44. Corma, A., Martínez, A., and Martínez, C., *J. Catal.* **164**, 422 (1996).
45. Okuhara, T., Nishimura, T., Watanabe, H., Na, K., and Misono, M., *in* "Studies in Surface Science and Catalysis 90: Acid-Base Catalysis II" (H. Hattori, M. Misono, and Y. Ono, Eds.), p. 419. Kodansha, Tokyo, 1994.
46. Okuhara, T., Nishimura, T., and Misono, M., *Chem. Lett.* 155 (1995).
47. Mizuno, M., Katamura, K., Yoneda, Y., and Misono, M., *J. Catal.* **83**, 384 (1983).
48. Eguchi, K., Toyozawa, Y., Furuta, K., Yamazoe, N., and Seiyama, T., *Chem. Lett.* 1253 (1981).
49. Tsunecki, H., Niiyama, H., and Echigoya, E., *Chem. Lett.* 645 (1978).
50. Akimoto, M., and Echigoya, E., *Chem. Lett.* 1579 (1981).
51. Tsunecki, H., Niiyama, H., and Echigoya, E., *Chem. Lett.* 1163 (1978).